A COMPUTATIONAL APPROACH TO PREDICTING THE OCCURRENCE OF LOCALIZED CORROSION IN MULTICOMPONENT AQUEOUS SOLUTIONS

A. Anderko
OLI Systems, Inc.
108 American Road
Morris Plains, NJ 07950

N. Sridhar, D.S. Dunn and C. S. Brossia
Southwest Research Institute
6220 Culebra Road
San Antonio, TX 78238

ABSTRACT

A general model has been developed for predicting the occurrence of localized corrosion in multicomponent electrolyte solutions. The model is based on calculating the repassivation and corrosion potentials as functions of solution composition and temperature. For the corrosion potential, a previously developed mixed-potential model is used. For the repassivation potential, a new model has been developed on the basis of nonequilibrium thermodynamics of metal dissolution within a pit or crevice. The model assumes that the status of localized corrosion is determined by competitive processes at the metal - salt film - solution interfaces leading to either metal salt or oxide formation. To calibrate and verify the model, an extensive database of repassivation potentials has been established for eleven alloys (UNS N06022, N10276, N06625, N08825, N06600, N06690, N08800, N08367, S31254, S31603 and S41425). The model successfully predicts the observed effects of aggressive species, such as chloride and bromide, inhibiting species, such as nitrate, and non-aggressive species, such as acetate, on the repassivation potential. A generalized correlation has been established to relate the repassivation potential to alloy composition. Further, the model has been validated by predicting the critical crevice temperature in $FeCl_3$ solutions.

Keywords: Localized corrosion, stainless steels, nickel-base alloys, repassivation potential, corrosion potential

INTRODUCTION

Localized corrosion is controlled by a multitude of factors such as the chemistry of the aqueous system, concentrations of components, temperature and alloy composition. Therefore, it is desirable to rationalize and predict the effects of these factors whenever a need arises to design chemical process equipment, mitigate existing corrosion problems, etc. Predicting localized corrosion based only on the knowledge of process parameters has been considered an impossible task until recently. However, advances in the understanding of parameters governing localized corrosion and the ability to calculate these parameters on the basis of thermophysical and electrochemical principles can open new possibilities for assessing the performance of an alloy once the process parameters are known. Although experimental and plant corrosion data are still the best guides for performance prediction, computational models can provide guidelines for process modifications or materials selection. The objective of this paper is to describe such a predictive model and verify it using well-defined experimental data. A separate paper will show the results of plant tests that further validate the model.

Localized corrosion occurs when the corrosion potential of an alloy in a given environment exceeds a critical potential[1]. While this concept is well accepted, the definition of critical potential is still debated. In the approach described in this paper, the repassivation potential is used as the critical potential for localized corrosion. The repassivation potential (also called the protection potential) is the potential at which a stably growing pit or crevice corrosion will cease to grow. The use of the repassivation potential is generally criticized on the basis of two lines of argument: (1) the measured repassivation potential decreases with an increase in pit depth and, because of this, the repassivation potential measured on shallow pits or by a relatively rapid scan rate cyclic potentiodynamic polarization (CPP) test may not be sufficiently conservative[2,3] and (2) the repassivation potential measured on deep pits may be too low and, therefore, unnecessarily conservative for predicting the occurrence of localized corrosion.

Experiments conducted by a number of investigators have shown that the repassivation potential does not decrease at a constant rate with pit or crevice depth. This is illustrated in Figure 1, which is a composite result of a number of alloy-environment combinations. The repassivation potential attains a lower-bound value as the pit or crevice depth increases (higher charge density). Alternatively, it may be argued that it has a logarithmic dependence with pit/crevice depth, which would result in insensitivity to pit depths at large values. Indeed, as shown in Figure 1, the original concern that short-term tests may produce a non-conservative predictive parameter[2,3] arose because the investigators used low charge densities (shallow pits) and did not consider crevice corrosion. Furthermore, for pits initiated rapidly at high potentials and repassivated at lower potentials, the time for repassivation increases as the repassivation potential is increased. This is illustrated for a Ni-base alloy, alloy 825, in Figure 2. Two different groups of specimens are shown in Figure 2. These two groups were created by holding the crevice sample at high potentials for different lengths of time to achieve different pit depths[4]. The pit depths were measured perpendicular to crevice surfaces. As the potential at which the crevices are repassivated increases, the time for repassivation also increases and, beyond a certain potential, repassivation does not occur within the experimental time. The repassivation time depends on the initial pit depth because the time for transport of species in and out of the pits increases with increasing pit depth. If the pit or crevice corrosion depth is maintained at a constant value, then slower scan rates lead to an increase in repassivation potential. Indeed, under these test conditions, rapid scan rates lead to an excessively conservative estimate of the repassivation potential. On the other hand, under potentiostatic conditions, the time required to initiate pitting and crevice corrosion increases when the potential is decreased towards the repassivation potential (Figure 2). Thus, if a specimen is held over long periods of

time at fixed potentials, the initiation and repassivation occur within the same range of potentials, which is a predictor of the long-term occurrence of localized corrosion.[5]

In this paper, we describe a new mechanistic model that can be used to predict the repassivation potential as a function of aqueous environment composition and temperature. When calibrated against a relatively small set of experimental data, this model is capable of predicting repassivation potentials in wide ranges of environments. The accuracy of the model is demonstrated by comparing the calculated repassivation potentials with experimental data for a number of combinations of components, including aggressive, non-aggressive and inhibitive species. Further, a correlation is developed to relate the repassivation potential to the composition of the alloy.

For the corrosion potential, a previously developed electrochemical model is used.[6-8] The simultaneous computation of the corrosion and repassivation potential for a given environment makes it possible to predict the long-term occurrence of localized corrosion. This will be demonstrated by predicting the critical crevice temperature and comparing it with experimental data.

EXPERIMENTAL APPROACH

The design of the experimental cell and electrodes has been described previously[5,9,10]. The crevice corrosion repassivation potential (E_{rcrev}) was measured using specimens fitted with a serrated crevice washer made of polytetrafluoroethylene (PTFE). Here, E_{rcrev} and the pitting repassivation potential (E_{rp}) are used interchangeably because, for deep pits, they were found to be equivalent.[5,9] Crevices were created on 3-mm thick (0.125 inches) sheet samples by clamping serrated polytetrafluoroethylene (PTFE) washers (12 teeth per side) using alloy C-276 (UNS N10276) bolts isolated through PTFE sleeves and an initial torque of 0.14 N.m (20 in. oz.). The samples were held potentiostatically at a more positive potential such that the current density increased with time at this potential, which was indicative of localized corrosion growth. Holding the potential at too high a value can lead to large currents, which are essentially constant with time.[8] In these cases, no localized corrosion is observed, the currents being indicative of transpassive dissolution and water breakdown.[11] After a fixed charge density is passed at high potentials, the potential is lowered at a slow scan rate of 0.167 mV/s. The repassivation potentials were defined as the potentials at which the current density corresponded to 10^{-2} A/m^2. The choice of the current density is arbitrary, and for most systems, does not result in significant discrepancy in E_{rcrev} because the current decreases rapidly with potential in this regime. As mentioned previously, at rapid backward scan rates, the repassivation potential is low and is too conservative for long-term prediction. At slow scan rates (less than 0.167 mV/s), the repassivation potential shows significant scatter.[11] The scan rate used above provided a good compromise between reproducibility and excessive conservatism.[11] For tests at or below 95°C, tests were conducted in glass kettles.[9] Tests above this temperature were conducted in PTFE-lined stainless steel autoclaves using an internal Ag/AgCl reference electrode. Repassivation potential data were obtained for eleven alloys (C-22, C-276, 625, 825, 600, 690, 800, AL6XN, 254SMO, 316L and super 13Cr).

COMPUTATIONAL MODEL

As outlined above, localized corrosion can be predicted to occur over the long-term when the corrosion potential exceeds the repassivation potential at the conditions of interest. Thus, a predictive computational model must calculate both the corrosion and repassivation potentials as functions of environmental conditions. In our previous papers, a comprehensive general corrosion model was developed for the computation of the corrosion potential as well as general corrosion rates as a function

of solution chemistry, temperature and flow conditions.[6-8,12] In the present work, we discuss a model for calculating the repassivation potential as a function of environmental conditions.

The concentration dependence of the pitting potential has been extensively studied in the literature. Several theories have been developed to relate the pitting potential to the activity of an aggressive solution species.[1] However, considerably less attention has been devoted to the concentration dependence of the repassivation potential. In this study, we adopt the conceptual approach developed by Okada[13] for the repassivation of a stable pit. Okada[13] assumed that a metal halide salt layer is present at the interface between the metal and pit solution in a stably growing pit. High metal dissolution rate and electromigration of halides are necessary to maintain the halide layer. Okada conceptualized that nuclei of metal oxide are formed within this halide layer as the potential approaches the repassivation potential. The dissolution rate of the metal through the oxide nucleus is assumed to be much slower than through the halide layer. Thus, as the potential approaches the repassivation potential, the oxide nucleus grows at the expense of the halide layer, which further reduces the kinetics of metal dissolution and stabilizes the oxide layer. This conceptual model is consistent with experimental observations of salt film formation at the bottom of active pits and the need to reduce the solution concentration in contact with the growing pit interface to a critical percentage of saturation concentration with respect to metal chloride salt so that repassivation could occur. Okada[13] used techniques of irreversible thermodynamics to derive conditions under which a metal oxide layer becomes stable in the process of repassivation at the interface between a metal and a metal halide. Okada's derivation yields a linear dependence of the repassivation potential on the logarithm of the activity of an aggressive ion X, i.e.,

$$E_{rp} = a + b \ln a_{X^-} \tag{1}$$

This function is analogous to that obtained by various authors for the pitting potential. However, eq. (1) is clearly incapable of reproducing the complex dependence of the repassivation potential on the concentration of aggressive ions. In particular, it does not reproduce the two distinct slopes of the repassivation potential dependence on the logarithm of the activity of chlorides.[5,11] Also, it cannot explain the drastic changes in the repassivation potential as inhibiting species are added to the system.[11] Therefore, it is necessary to develop a more comprehensive functional relationship that could relate the repassivation potential to the solution chemistry in a more realistic way. In a previous study,[14] a model was developed for relating the pitting potential (E_{pit}) to the activities of species in multicomponent solutions. This model successfully reproduced the complex composition dependence of the pitting potential of aluminum in solutions containing chlorides, perchlorates, sulfates and nitrates. Although this model was derived strictly for the pitting potential,[14] the functional form of the dependence of E_{pit} on solution composition was also found to be suitable for correlating the composition dependence of the repassivation potential. However, such an extension did not have a firm theoretical basis. In this study, we derive a model that is specifically designed to relate the repassivation potential to solution chemistry.

For this purpose, we consider a system that consists of the phases illustrated in Figure 3. In this system, the metal M undergoes dissolution underneath a layer of a nonprotective hydrous halide MX of thickness l. This thickness is assumed to be much smaller than the size of the pit so that the system can be regarded as one-dimensional. The MX phase dissolves in the solution within a boundary layer of thickness Δ. In the process of repassivation, a thin layer of oxide may form at the interface between the metal and the hydrous metal halide. We assume that, at a given instant, the oxide layer covers a certain fraction of the metal surface. This surface coverage fraction is denoted by θ_{ox}. This physical scheme is similar to that proposed by Okada[13], but it introduces the additional concept of the partial coverage fraction by the metal oxide monolayer. The measurable potential drop across the interface can be then expressed as a sum of four contributions, i.e.,

$$E = \Delta\Phi_{M/MX}(1,2) + \Delta\Phi_{MX}(2,3) + \Delta\Phi_{MX/S}(3,4) + \Delta\Phi_{S}(4,5) \tag{2}$$

where $\Delta\Phi_{M/MX}(1,2)$ is the potential difference at the interface between the metal and metal halide, which may be influenced by the partial coverage by the metal oxide, $\Delta\Phi_{MX}(2,3)$ is the potential drop across the hydrous halide layer, $\Delta\Phi_{MX/S}(3,4)$ is the potential difference across the metal halide/solution interface and $\Delta\Phi_S(4,5)$ is the potential drop across the boundary layer within the solution. The numbers in parentheses denote the interfaces as depicted in Figure 3.

At the metal/metal halide interface, the total current density can be expressed as a sum of the contributions of an active dissolution current, which leads to the formation of metal ions, and a current that leads to the formation of the oxide. These two contributions to the current are denoted by i_1 and i_2, respectively. They are both functions of $\Delta\Phi_{M/MX}(1,2)$. Taking into account that the fraction of the surface covered by the oxide layer is θ_{ox}, the total current density across the (1,2) interface is expressed as

$$i = \left[i_1(\Delta\Phi_{M/MX}(1,2)) + i_2(\Delta\Phi_{M/MX}(1,2))\right](1-\theta_{ox}) \tag{3}$$

The change of the oxide coverage fraction results from the competition between the formation of the oxide and its dissolution. Since the rate of formation of the oxide is proportional to $(1-\theta_{ox})$ and the rate of oxide dissolution is proportional to θ_{ox}, we have

$$\frac{\partial\theta_{ox}}{\partial t} = ci_2(\Delta\Phi_{M/MX}(1,2))(1-\theta_{ox}) - k\theta_{ox} \tag{4}$$

Solving eq. (4) in the steady-state limit (i.e., $\partial\theta_{ox}/\partial t \to 0$ as $t \to \infty$) and substituting the result into eq. (3), we obtain a relationship between the measurable current density and the potential difference $\Delta\Phi_{M/MX}(1,2)$:

$$i = \frac{i_1(\Delta\Phi_{M/MX}(1,2)) + i_2(\Delta\Phi_{M/MX}(1,2))}{1 + \dfrac{ci_2(\Delta\Phi_{M/MX}(1,2))}{k}} = \frac{i_1(\Delta\Phi_{M/MX}(1,2)) + i_2(\Delta\Phi_{M/MX}(1,2))}{1 + \dfrac{i_2(\Delta\Phi_{M/MX}(1,2))}{i_p}} \tag{5}$$

where the ratio k/c constitutes the passive current density i_p.

To obtain a relationship between the current density and the potential drop across the hydrous halide layer, $\Delta\Phi_{MX}(2,3)$, we use a simplified expression for the flux of species through the halide layer, which was derived by Okada[13] using nonequilibrium thermodynamics:

$$J_j' = \overline{n_j'}\,\overline{v_j'}\,\Delta\tilde{\mu}_j' \tag{6}$$

where $\overline{n_j'}$ is the mean concentration of species in the hydrous halide, $\overline{v_j'}$ is the mean mobility of species j per unit force and $\Delta\tilde{\mu}_j'$ is the gradient of the electrochemical potential, which is given by

$$\Delta\tilde{\mu}_j' = \frac{\mu_j(2) - \mu_j(3)}{l} + \frac{z_j F\Delta\Phi_{MX}(2,3)}{l} \tag{7}$$

where $\mu_j(2)$ and $\mu_j(3)$ are the chemical potentials of species j within the hydrous halide at the interfaces with the metal and the solution, respectively. In the particular case of metal ions M, the steady-state flux J_M' is determined by the combined effect of the current that results in the formation of metal ions and the flux that results from the dissolution of the metal oxide. The current that results in the formation of metal ions is $i_1(1-\theta_{ox})$. The current that results from the dissolution of the oxide is equal to $i_p\theta_{ox}$.

From eq. (4), we obtain $i_p \theta_{ox} = (k/c)\theta_{ox} = i_2(1-\theta_{ox})$ as $\partial\theta_{ox}/\partial t \to 0$. Thus, the flux of metal ions is given by

$$J_i' = \frac{i_1(1-\theta_{ox})+i_p\theta_{ox}}{z_M F} = \frac{i_1(1-\theta_{ox})+i_2(1-\theta_{ox})}{z_M F} = \frac{i}{z_M F} \tag{8}$$

where i is given by eq. (5). By applying eqs. (6) and (7) to metal ions (i.e., for $j = M$) and utilizing eq. (8), we obtain a relationship between the potential drop across the metal halide layer and the steady-state current density:

$$\Delta\Phi_{MX}(2,3) = \frac{il}{z_M^2 F^2 \overline{n_M' v_M'}} - \frac{\mu_M(2)-\mu_M(3)}{z_M F} \tag{9}$$

At the metal halide/solution interface (3,4), we can assume equilibrium between the formation and dissolution of the metal halide. Hence,

$$\tilde{\mu}_j(3) = \tilde{\mu}_j(4) \tag{10}$$

Since $\tilde{\mu}_j = \mu_j + z_j F\Phi$, a rearrangement of eq. (10) for $j = M$ yields a relationship for the potential drop across the metal halide/solution interface:

$$\Delta\Phi_{MX/S}(3,4) = \frac{\mu_M(4)-\mu_M(3)}{z_M F} \tag{11}$$

For the flux of species through the solution boundary layer (4,5), we use the simplified expression that was obtained by Okada[13] from nonequilibrium thermodynamics:

$$J_j'' = \overline{C_j'' v_j''}\Delta\tilde{\mu}_j'' \tag{12}$$

where $\overline{C_j''}$ is the mean concentration of species j, $\overline{v_j''}$ is the mean mobility and the gradient of the electrochemical potential $\Delta\tilde{\mu}_j''$ is given by

$$\Delta\tilde{\mu}_j'' = \frac{\mu_j(4)-\mu_j(5)}{\Delta} + \frac{z_j F\Delta\Phi_S(4,5)}{\Delta} \tag{13}$$

Since the flux of metal ions in the steady state is given by

$$J_M'' = \frac{i}{z_M F}, \tag{14}$$

the potential drop across the boundary layer can be obtained from eqs. (12) and (13) with $j = M$ and eq. (14) as

$$\Delta\Phi_S(4,5) = \frac{i\Delta}{z_M^2 F^2 \overline{C_M'' v_M''}} - \frac{\mu_M(4)-\mu_M(5)}{z_M F} \tag{15}$$

By substituting eqs. (9), (11) and (15) into eq. (2), we obtain the following expression for the potential:

$$E = \Delta\Phi_{M/MX}(1,2) + \frac{i}{z_M^2 F^2}\left[\frac{l}{\overline{n_M' v_M'}} + \frac{\Delta}{\overline{C_M'' v_M''}}\right] + \frac{\mu_M(5)-\mu_M(2)}{z_M F} \tag{16}$$

It should be noted here that the thickness of the salt film l adjusts to accommodate the potential. In principle, a mathematical analysis of the conditions that lead to a stable film thickness can be performed by minimizing the entropy production as the system tends towards the steady state. Okada[13] developed such conditions for the thickness of the passive film formed during repassivation. Similar methodology can be applied to the thickness of the salt film. However, this would be beyond the scope of this paper.

In eq. (16), the quantity in brackets is approximately constant for a given system and will be denoted by K. Since the chemical potential of the metal is related to the metal activity by $\mu_M = \mu_M^0 + RT \ln a_M$, eq. (16) can be rewritten as

$$E = \Delta\Phi_{M/MX}(1,2) + \frac{Ki}{z_M^2 F^2} + \frac{RT}{z_M F} \ln \frac{a_M(5)}{a_M(2)} \tag{17}$$

In the next step, we consider the relationship between the activities of electrochemically active species (e.g., halide ions) at the metal surface (2) and the potential drop between the metal surface (2) and the bulk solution (5). The flux of active species through the hydrous halide can be calculated from eqs. (6) and (7). Similarly, eq. (10) holds for the active species and their flux through the boundary layer can be represented by eqs. (12) and (13). Thus, the potential drop between (2) and (5) can be related to the chemical potentials of the active species at the metal surface (2) and in the bulk of the solution by

$$\Delta\Phi_{MX}(2,3) + \Delta\Phi_{MX/S}(3,4) + \Delta\Phi_S(4,5) = \frac{J_j' l}{z_j F \overline{n_j' v_j'}} + \frac{J_j'' \Delta}{z_j F \overline{C_j'' v_j''}} + \frac{\mu_j(5) - \mu_j(2)}{z_j F} \tag{18}$$

where J_j' and J_j'' are the fluxes of the active species j through the metal halide and the solution boundary layer, respectively. Using activities rather than chemical potentials for the species j and considering that the potential drop between (2) and (5) is also given by the last two terms of eq. (17), we obtain a relationship for the activity of the reactive ions at the metal surface:

$$\frac{RT}{z_j F} \ln \frac{a_j(5)}{a_j(2)} = \frac{Ki}{z_M^2 F^2} + \frac{RT}{z_M F} \ln \frac{a_M(5)}{a_M(2)} - \frac{J_j' l}{z_j F \overline{n_j' v_j'}} - \frac{J_j'' \Delta}{z_j F \overline{C_j'' v_j''}} \tag{19}$$

Thus, the state of the system is described by three relationships, i.e., (i) eq. (17), which determines the measurable potential; (ii) eq. (5), which provides an expression for the total current density and (iii) eq. (19), which relates the activities of the reactive species at the metal interface and in the bulk solution.

On the basis of these relationships, we can now consider the limiting behavior of the system as repassivation is approached. In experiments, the repassivation potential is typically defined when the current density reaches a certain small value $i = i_{rp}$ (e.g., $i_{rp} = 10^{-2}$ A/m^2). Then, the term $Ki/z_M^2 F^2$ becomes equal to a certain constant value $Ki_{rp}/z_M^2 F^2$. Also, as repassivation is reached, the activity of the metal ions at the metal surface, $a_M(2)$, becomes lower and close to the value resulting from passive dissolution, which is a constant at fixed external conditions. Assuming that the activity of metal ions in the bulk solution is equal to some small, fixed value (which is typically the case in most experiments and practical applications), the term $\frac{RT}{z_M F} \ln \frac{a_M(5)}{a_M(2)}$ becomes a constant. Then, eq. (17) can be rewritten for the special case of the repassivation potential ($E = E_{rp}$) as:

$$E_{rp} = \Delta\Phi_{M/MX}(1,2) + K_1 \tag{20}$$

where K_1 is a constant. In eq. (20), the fluxes of the active species become very small at the stage of repassivation and become comparable to the flux of the metal that results from passive dissolution. Then, eq. (19) can be simplified as

$$\frac{RT}{z_j F} \ln \frac{a_j(5)}{a_j(2)} \approx K_2, \tag{21}$$

Eq. 21 yields a simple relationship between $a_j(5)$ and $a_j(2)$, i.e.,

$$\frac{a_j(5)}{a_j(2)} \approx \exp\left(\frac{z_j F K_2}{RT}\right) = K_3 \tag{22}$$

These limiting functions will be later shown to be useful for deriving a closed-form expression for the repassivation potential.

In the next step, we develop relationships between the current densities i_1 and i_2 (cf. eq. 5) and the solution chemistry. In general, we consider a system in which multiple electrochemically active (either aggressive or inhibitive) species may be present. To take into account multiple solution species, we consider competitive adsorption of species at the metal surface (2), i.e.,

$$\equiv M + X^{(j)} = \equiv MX^{(j)}, \tag{23}$$

The adsorption is characterized by the partial surface coverage fractions $\theta_j(2)$, which are related to the activities of the species at the metal surface $a_j(2)$. The adsorption is followed by the dissolution of the adsorbed complex:

$$\equiv MX^{(j)} \to M^{z+} + X^{(j)} + ze^- \tag{24}$$

The current density that is associated with the dissolution of the j-th complex in the active state can be expressed by the following expression (cf., Popov and Sidorenko[15]):

$$i_{1,j} = k_j'\left(\theta_j(2)\right)^{n_j} \exp\left(\frac{\alpha_j F \Delta\Phi_{M/MX}(1,2)}{RT}\right) \tag{25}$$

where n_j is the reaction order with respect to species j. The current density for the active dissolution of multiple complexes is given by the sum of the contributions given by eq. (25), i.e.,

$$i_1 = \sum_j k_j'\left(\theta_j(2)\right)^{n_j} \exp\left(\frac{\alpha_j F \Delta\Phi_{M/MX}(1,2)}{RT}\right) \tag{26}$$

At repassivation, the potential difference $\Delta\Phi_{M/MX}(1,2)$ is related to the repassivation potential by eq. (20). Then, eq. (26) takes a limiting form, i.e.,

$$i_1 = \sum_j k_j'\left(\theta_j(2)\right)^{n_j} \exp\left(\frac{\alpha_j F(E_{rp} - K_1)}{RT}\right) = \sum_j k_j''\left(\theta_j(2)\right)^{n_j} \exp\left(\frac{\alpha_j F E_{rp}}{RT}\right) \tag{27}$$

The current density that leads to the formation of an oxide layer (i.e., i_2 in eq. 5) also results from the adsorption of species at the metal surface. However, the species that are responsible for the formation of the oxide are different from those that facilitate active dissolution. As pointed out by Okada[13], a reaction of water molecules with the metal surface is a prerequisite for repassivation. In addition to water molecules, various inhibitive species may adsorb at the metal surface and promote the formation of an oxide. Thus, the current density i_2 can be represented by an equation that is formally analogous to eq. (25) and, hence, also to eq. (27) in its mathematical form, i.e.,

$$i_2 = \sum_j l_j'\left(\theta_j(2)\right)^{n_j} \exp\left(\frac{\xi_j F \Delta\Phi_{M/MX}(1,2)}{RT}\right) = \sum_j l_j''\left(\theta_j(2)\right)^{n_j} \exp\left(\frac{\xi_j F E_{rp}}{RT}\right) \tag{28}$$

where ξ_j denotes the electrochemical transfer coefficient for a reaction mediated by an inhibitive species. However, the summation in eq. (28) is performed over different species than those in eq. (27). Specifically, water is the first species in eq. (28) since it contributes to the formation of the oxide. The remaining species in eq. (28) are inhibiting species such as nitrates, chromates, etc.

To relate the surface coverage fractions $\theta_j(2)$ to the solution chemistry, it is necessary to use an adsorption isotherm. To a first approximation, the surface coverage fraction can be expressed using a Langmuir model, i.e.,

$$\theta_j(2) = \frac{r_j' a_j(2)}{1 + \sum_k r_k' a_k(2)} \tag{29}$$

Since, at the repassivation potential, the activity of the species j at the metal surface (2) is related to the activity in the bulk solution (5) by eq. (22), we have

$$\theta_j(2) = \frac{r_j' \dfrac{a_j(5)}{K_2}}{1 + \sum_k r_k' \dfrac{a_k(5)}{K_2}} = \frac{r_j a_j(5)}{1 + \sum_k r_k a_k(5)} \tag{30}$$

where the coefficient r_j is a scaled adsorption constant. In the limit of repassivation, eq. (5) for the total current density becomes

$$i_{rp} = \frac{i_1(E_{rp}) + i_2(E_{rp})}{1 + \dfrac{i_2(E_{rp})}{i_p}} \tag{31}$$

where i_{rp} is the value of the current density at which the repassivation potential is measured and the contributions $i_1(E_{rp})$ and $i_2(E_{rp})$ are given by eqs. (27) and (28), respectively. The contributions $i_1(E_{rp})$ and $i_2(E_{rp})$ can be calculated using the partial coverage fractions obtained from eq. (30).

Substitution of eqs. (27) and (28) into eq. (31) yields an equation that can be solved numerically to obtain the value of the repassivation potential:

$$1 + \sum_j \left[\left(\frac{i_{rp}}{i_p} - 1 \right) \frac{l_j''}{i_{rp}} \right] \theta_j^{n_j} \exp\left(\frac{\xi_j F E_{rp}}{RT} \right) = \sum_j \frac{k_j''}{i_{rp}} \theta_j^{n_j} \exp\left(\frac{\alpha_j F E_{rp}}{RT} \right) \tag{32}$$

where the symbol θ_j is used instead of $\theta_j(2)$ for simplicity. The summation on the left-hand side of eq. (32) is performed over water and inhibitive species whereas the sum on the right-hand side is calculated over the aggressive species. In Appendix A, simplified forms of eq. (32) are given for three practically important special cases, i.e. for a metal in contact with (i) one aggressive species (e.g., chloride) in an aqueous solution; (ii) two aggressive species (e.g., chloride and bromide) and (iii) an aggressive and an inhibitive species (e.g., chloride and nitrate).

The relationships described above have been derived for a repassivation process that occurs beneath a salt film. However, the presence of a salt film is not a limiting factor that determines the applicability of the model. Essentially the same final expressions can be derived when the environment within the pit or crevice is concentrated, but not necessarily at saturation. This is important in view of the fact that experimentally determined critical solution concentrations are often close to, but less than saturation.

9

Practical implementation of the model

As seen in eq. (32), some of the model parameters can be conveniently grouped to reduce the number of adjustable parameters. In addition, we can make two simplifying assumptions, i.e., the electrochemical transfer coefficients for aggressive species (α_i) can be assumed to be equal to one and the reaction orders for the effects of inhibiting species (n_j) can be assigned a default value of one. With these simplifications, eq. (32) contains the following parameters:

(1)   Scaled rate constant for aggressive ions, which can be expressed using a scaled Gibbs energy of activation $\Delta g^{\neq}_{A,j}$:

$$k_j = \frac{k_j{''}}{i_{rp}} = \exp\left(-\frac{\Delta g^{\neq}_{A,j}}{RT}\right) \tag{33}$$

(2)   Scaled rate constant for inhibitive species, which is also expressed using a scaled Gibbs energy of activation $\Delta g^{\neq}_{I,j}$:

$$\left(\frac{i_{rp}}{i_p}-1\right)\frac{l_j{''}}{c} = \exp\left(-\frac{\Delta g^{\neq}_{I,j}}{RT}\right) \tag{34}$$

(3)   Reaction order with respect to aggressive ions, n_j and

(4)   Electrochemical transfer coefficients for the inhibitive species, ξ_j.

(5)   Scaled Gibbs energy of adsorption $\Delta G_{ads,i}$, which defines the adsorption coefficient in eq. (30):

$$r_j = \exp\left(-\frac{\Delta G_{ads,j}}{RT}\right) \tag{35}$$

However, the latter property can be assigned a common default value for almost all species, including halide ions, and needs to be adjusted only for the metal/species combinations that show very strong specific effects.

The scaled Gibbs energies of activation may be further related to temperature as

$$\frac{\Delta g^{\neq}_{A,j}}{T} = \frac{\Delta g^{\neq}_{A,j}(T_{ref})}{T_{ref}} + \Delta h^{\neq}_{A,j}\left(\frac{1}{T}-\frac{1}{T_{ref}}\right) \tag{36}$$

and

$$\frac{\Delta g^{\neq}_{I,j}}{T} = \frac{\Delta g^{\neq}_{I,j}(T_{ref})}{T_{ref}} + \Delta h^{\neq}_{I,j}\left(\frac{1}{T}-\frac{1}{T_{ref}}\right) \tag{37}$$

RESULTS AND DISCUSSION

First, we apply the model to study the effect of solution chemistry on the repassivation potential. For this purpose, we calculate the repassivation potentials of one selected alloy (type 316L stainless steel) in the presence of aggressive, non-aggressive and inhibitive ions. Then, we analyze the behavior of various alloys in chloride solutions and develop a generalized correlation for the model parameters in terms of alloy composition. Finally, we combine the calculated repassivation and corrosion potentials to predict the critical crevice temperature in $FeCl_3$ solutions.

Effects of solution chemistry

The primary advantage of using a computational model lies in being able to predict the behavior of multicomponent systems based on experimental information for simpler systems that contain a limited number of electrochemically active species. The model developed in this study is of a semi-empirical nature, i.e., it requires the use of certain parameters that can be obtained only from experimental data. Such parameters should be determined from data for simple systems that contain one or two active anions. Then, if the model is physically sound, the same parameters will be applicable to multicomponent systems. Therefore, to verify the model, we apply it to:

(a) Alloys in contact with chlorides as the most common and practically important aggressive species.

(b) Alloys in contact with chlorides and bromides, which exemplify a mixture of two aggressive ions. In this case, repassivation potential is expected to increase gradually as a less aggressive species is substituted for a more aggressive species.

(c) Alloys in contact with chlorides and selected non-aggressive anions, including acetates, nitrates and sulfates. In this case, the mildly inhibitive species act to dilute the aggressive species. The repassivation potential is expected to increase slightly with increasing concentration of the inhibitive species, but when the inhibitor concentration reaches a high value such that there is essentially a very small concentration of the aggressive species, the repassivation potential rises steeply. In the case of solutions with a strong inhibitor, the repassivation potential rises steeply at a much smaller concentration of the inhibitor species than in the previous case.

(d) Alloys in contact with solutions containing three different anions.

For these four cases, the model predictions are compared to repassivation potentials generated as part of the current study. An important test of the model is to predict the behavior of a system made up from a combination of aggressive, weakly inhibitive, and strongly inhibitive species.

Figure 4 shows the calculated and experimental repassivation potentials for type 316L stainless steel in chloride solutions at two temperatures. In Figures 4, the chloride activity was calculated for various molalities of NaCl using the thermodynamic model described in previous papers.[6-8] As shown in these figures, the slope of the repassivation potential changes as a function of chloride activity. This is a general phenomenon for alloys. However, the transition between the low-slope and high-slope segments of the curves strongly depends on the alloy and temperature. For less corrosion-resistant alloys such as type 304L stainless steel, the transition may occur at very low chloride concentrations and only a single logarithmic slope is generally reported. The low-slope portion of the curve at higher chloride activities is determined by the parameters that represent the dissolution of the metal through the formation of metal-chloride complexes (i.e., $\Delta g^{\neq}_{A,Cl}$ and n_{Cl}). The steeper portion at lower chloride concentrations is additionally determined by the parameters that represent the formation of the oxide through a reaction with water molecules (i.e., $\Delta g^{\neq}_{I,H2O}$ and ξ_{H2O}). The slope of this segment increases with an increase in the parameter ξ_{H2O}. The model represents the data essentially within experimental uncertainty.

For an additional verification of the repassivation potential model, it is of interest to examine the current density versus potential relationship as the repassivation potential is approached. As described above, the repassivation potential model has a limiting character, i.e., it reaches a closed algebraic form as the potential approaches the repassivation potential. Thus, the predicted current density versus potential relationship should be in agreement with experimental data in the repassivation limit. To make a comparison with experimental *i(E)* data, eqs. (23), (19) and (20) were used for potentials increasingly

deviating from E_{rp} (i.e., for $E \geq E_{rp}$). For this purpose, the kinetic constant k_{Cl}'' was recalculated from the scaled activation energy $\Delta g^{\neq}_{A,Cl}$ using eq. (25) on the assumption that the repassivation potential is measured at the value of the current $i_{rp} = 10^{-2}$ A/m². Similarly, the constant l_{H2O}'' was recalculated from the $\Delta g^{\neq}_{I,H2O}$ parameter using eq. (26), the i_{rp} value and the value of the passive current density i_p obtained from the previously developed general corrosion model.[6-8] A comparison with experimental data is shown in Figure 5 for type 316L stainless steel in contact with selected chloride solutions. In this figure, the experimental points correspond to reverse CPP scans, which were also used to determine the repassivation potential. It should be noted that the experimental i vs. E relationships were not used to calibrate the parameters of the model. As shown in Figure 5, the model correctly predicts the limiting $i(E)$ slopes as the potential approaches E_{rp} and the current density approaches $i_{rp} = 10^{-2}$ A/m². At potentials substantially above E_{rp}, the predicted curves increasingly deviate from the data, which is expected in view of the limiting character of the model.

After calibrating the model for chloride systems, the repassivation potentials were calculated for solutions containing two aggressive ions, i.e., chlorides and bromides. The results of calculations are shown in Figure 6, which illustrates the variation in the repassivation potential as the relative amounts of chlorides and bromides are changed while keeping the total concentration of anions equal to 0.42 M. Bromide is generally not as aggressive as chloride in inducing localized corrosion. Therefore, the small increase in repassivation potential as one moves from a pure chloride solution to a pure bromide solution is understandable. The model needs to be calibrated only for pure aggressive ions, i.e., separately for chloride and bromide solutions. Then, the model predicts the repassivation potentials in mixed systems within experimental uncertainty as shown in Figure 6.

Repassivation potentials cannot be defined in solutions containing only non-aggressive ions because such ions do not induce localized corrosion. Therefore, the influence of non-aggressive ions on E_{rp} can be studied only in conjunction with aggressive ions. The effect of a non-aggressive anion X is determined by the parameters that represent the contribution of this anion to the formation of the oxide (i.e., $\Delta g^{\neq}_{I,X}$ and ξ_X). In the case of strongly inhibitive anions (such as nitrates), the $\Delta g^{\neq}_{I,X}$ parameter is negative or weakly positive, which corresponds to an appreciable value of the kinetic constant l_X''. In the case of weakly inhibitive ions, $\Delta g^{\neq}_{I,X}$ is strongly positive and l_X'' is small. In the extreme case of electrochemically inactive ions, l_X'' is equal to zero and such ions can be regarded as diluents.

Figure 7 shows the application of the model to systems containing chlorides as aggressive ions and acetates as weakly inhibitive ions. In this case, the repassivation potential rises steeply close to the pure acetate limit. The model accurately represents this behavior. For pure acetate ions, the experimental point corresponds to transpassive dissolution rather than localized corrosion. Since the values calculated from the E_{rp} model reflect localized corrosion, they tend to infinity as the pure acetate limit is approached.

The combined effect of nitrate and chloride ions is shown in Figure 8 for three levels of chloride concentrations. The presence of nitrates causes a steep increase in the repassivation potential at a certain nitrate concentration. This is a manifestation of the inhibitive properties of nitrate ions. The threshold concentration depends on the concentration of chloride ions. This behavior is quantitatively reproduced by the model as shown in Figure 9. It has been shown that for a given chloride concentration, the concentration of nitrate needed to inhibit localized corrosion depends on the Cr and Mo concentrations of the alloy. This may arise out of the dependence of $\Delta g^{\neq}_{I,NO_3^-}$ on the alloy chemistry and will be considered in a future study.

To verify the model for multicomponent solutions, tests were made for a mixed system containing chlorides, nitrates and acetates. It should be noted that experimental data for this multicomponent system were not used to calibrate the parameters of the model. Thus, the

multicomponent system provides a stringent test of the model. As shown in Figure 9, the repassivation potentials in this system are accurately predicted. The weakly inhibitive acetate ions shift the repassivation potential towards higher values. In view of the model, this is primarily due to the displacement of the chloride ions by acetate ions in a competitive adsorption process.

Effect of alloy composition

It is well known that the localized corrosion resistance of Fe-Ni-Cr-Mo alloys depends on a combination of the concentrations of Cr, Mo, W, and N. The Pitting Resistance Equivalence (PRE) used to characterize an alloy's relative performance ranking in a localized corrosion environment, involves a number of empirically derived equivalent compositions.[23] These alloy equivalents are limited to the experimental conditions and the range of alloys considered.[24] The modeling approach outlined above, enables one to rank the alloys in a wide range of user-specified environments. To obtain a quantitative understanding of the effect of alloy composition on the repassivation potential, experimental data for twelve alloys (UNS N06022, N10276, N06625, N08825, N06600, N06690, N08800, N08367, S31254, S31603, S30403 and S41425) have been analyzed. First, model parameters were determined for individual alloys. Then, the regularities of the parameters were analyzed to develop a correlation between model parameters and the composition of alloys from the Fe-Ni-Cr-Mo-W-N family. Such a correlation may be useful in practice since it makes it possible to predict the repassivation potentials for metals that have not been included in the experimental program.

A preliminary correlation has been established for systems containing aqueous chloride solutions because such systems are of primary practical significance and they have been experimentally investigated for a sufficiently large number of metals. The parameters of the correlation have been established using data for ten alloys (UNS N06022, N10276, N06625, N08825, N06600, N08367, S31254, S31603, S30403 and S41425). Subsequently, it was tested by comparing predicted and experimental repassivation potentials for alloys N06690 and N08800.

A system containing water and chloride ions is characterized, in the most general case, by seven parameters, i.e.,

(1) The parameters characterizing the dissolution reaction mediated by chloride ions, i.e., $\Delta g^{\neq}_{A,Cl}(T_{ref})$, $\Delta h^{\neq}_{A,Cl}$ and $n_{A,Cl}$.

(2) The parameters characterizing the formation of oxide as a result of a reaction with water, i.e., $\Delta g^{\neq}_{I,H2O}(T_{ref})$, $\Delta h^{\neq}_{I,H2O}$ and $\xi_{I,H2O}$. These parameters remain independent of the ionic species in the solution.

(3) A parameter characterizing the adsorption of chloride ions, i.e., $\Delta G_{ads,Cl}$.

This seemingly large number of parameters is not a hindrance to develop a general treatment because the parameters show significant regularities. In particular, three parameters can be assigned universal values without any loss in accuracy. The Gibbs energy of adsorption of ions can be set equal to a common value, i.e.,

$$\Delta G_{ads,Cl} /(kJ / mol) = 10 \tag{38}$$

Further, based on the analysis of experimental data, it was determined that the steeper portion of the plot of repassivation potential versus chloride activity has similar slopes for various metals. Therefore, the electrochemical transfer coefficient for the formation of oxides as a result of reaction with water can be assigned a common value, i.e.,

13

$$\xi_{I,H_2O} = 0.9 \tag{39}$$

Further, the $n_{A,Cl}$ parameter was found to have an approximately constant value, i.e.,

$$n_{A,Cl} = 1.3 \tag{40}$$

The remaining parameters depend on the composition of the metal. The enthalpy of activation for the dissolution mediated by chloride ions was found to be related to the main components of the passivating oxides, i.e., Cr, Mo and W:

$$\Delta h_{A,Cl}^{\neq} /(kJ/mol) = 0.01 + (x_{Mo} + x_W)^8 x_{Cr}^{16} \tag{41}$$

where x_i is the mole fraction of the metal component i. The Gibbs energy of activation for the same reaction is given by

$$\Delta g_{A,Cl}^{\neq} /(kJ/mol) = -66.402 + 134.55 x_{Cr}^{0.705} \left(1 + 3.225(x_{Mo} + x_W)^{0.443}\right) - 2.1e4 x_N (x_{Mo} + x_W) - 460.9 x_{Nb} \tag{42}$$

In comparison with the enthalpy of activation, the Gibbs energy of activation involves the dependence on the mole fraction of N and Nb. The dependence on the Nb mole fraction is very tentative because it is based on only one alloy (alloy 625).

For the oxide formation as a result of a reaction with water, the activation enthalpy is correlated with $\Delta g_{A,Cl}^{\neq}$:

$$\Delta h_{I,H_2O}^{\neq} (kJ/mol) = 0.0012 \Delta g_{A,Cl}^{\neq} + 0.015 \tag{43}$$

The Gibbs energy of activation for this reaction is given by

$$\Delta g_{I,H_2O}^{\neq} (kJ/mol) = 9.01 + 537.1 x_{Cr}^3 + 41.85(x_{Mo} + x_W)^{1/3} - 605 x_{Nb} \tag{44}$$

As with eq. (42), the last term in eq. (44) is tentative.

The repassivation potentials calculated from the generalized correlation (eqs. 38 through 44) are shown in Figures 10 through 11 for several alloys in chloride solutions at 296 K, 333K, 368 K and 423 K, respectively. The majority of experimental data points shown in these figures were obtained as part of the current research program. The only exception is UNS S30403, for which the data of Yashiro et al.[16] were used. The overall average deviation between calculated and experimental data for all alloys is 74 mV. This can be compared with the average deviation of 40 mV, which is obtained when repassivation potential data are fitted separately for each alloy. Thus, the generalized correlation increases the overall deviation only from 40 to 74 mV. After the correlation has been established, it has been tested using the newly obtained data for alloys UNS N06690 and UNS N08800 at 333 K. The results of prediction are included in Figure 11. Although the data for alloys UNS 6690 and N08800 were not used to develop the generalized correlation, the predicted repassivation potentials agree well with experimental data.

Prediction of the critical crevice temperature

Critical crevice temperature (CCT) is a convenient measure of relative corrosion resistance of alloys in oxidizing chloride environments such as $FeCl_3$ solutions. The repassivation potential model described in this study, coupled with the previously developed general corrosion model, can be used to predict the critical crevice temperature. At temperatures below CCT, the calculated corrosion potential (E_{corr}) should lie below the repassivation potential (E_{rp}) whereas it should exceed E_{rp} above CCT. Thus, the intersection of the E_{corr} and E_{rp} curves versus temperature should provide an estimate of CCT.

Figure 14 shows the dependence of the calculated corrosion and repassivation potentials on temperature for alloy UNS N06022 in 6% $FeCl_3$ solutions. The corrosion potential was calculated using the previously developed general corrosion model,[6-8] in which the exchange current densities for the reduction of Fe^{3+} ions were calibrated using the data of Kolts and Sridhar.[17] As shown in Figure 14, the repassivation potential substantially decreases with temperature whereas the corrosion potential slightly increases. The E_{rp} and E_{corr} curves intersect at 57 °C, which is in good agreement with the experimental critical crevice temperature obtained by Hibner.[18]

SUMMARY

A general model has been developed for predicting the localized corrosion repassivation potential in multicomponent electrolyte solutions. The model is based on a nonequilibrium thermodynamic treatment of competitive reactions of various species leading to the formation of oxide within a metal salt film. The model has been successfully used for predicting the repassivation potential for a large number of Fe-Ni-Cr-Mo-W alloys in aqueous environments. The calculated values are in good agreement with experimental data. Specifically, the model has been successfully validated for solutions containing various combinations of species, such as two aggressive species, an aggressive and a non-aggressive species or an aggressive and an inhibitive species. The advantage of the model is that it needs a small set of experimental data to predict the localized corrosion behavior in a large set of environments. Further, a preliminary correlation has been established between the model parameters and the composition of the alloy. This correlation was developed using experimental data for ten nickel-base alloys and stainless steels in chloride solutions. Then, it has been verified using experimental data for two additional alloys that were not included in the original database. In a future study, the correlation will be extended to include the effect of species other than chlorides.

The new repassivation potential model can be used to predict the long-term occurrence of localized corrosion. For this purpose, the predicted repassivation potential is compared with the corrosion potential, which is computed for the same environmental conditions using a previously developed electrochemical model of general corrosion. This approach has been successfully verified by predicting the critical crevice temperature in $FeCl_3$ solutions. The combined model has been implemented in software that can be used as a tool for understanding and predicting the effect of environmental variables on localized corrosion.

ACKNOWLEDGEMENT

REFERENCES

1.   Z. Szklarska-Smialowska, "Pitting Corrosion of Metals," National Association of Corrosion Engineers, Houston 1986.

2.   B.E. Wilde and E. Williams, J. Electrochemical. Soc., 118 (1971) 1057.

3.   B.E. Wilde, in "Localized Corrosion," R.W. Staehle and B.F. Brown, J. Kruger, and A. Agarwal (ed.), Houston, TX: NACE International, 1974, p. 342.

4.   N. Sridhar, D.S. Dunn, C.S. Brossia, and G.A. Cragnolino, in: G. Frankel (Ed.), Localized Corrosion, Research Topical Symposium, Corrosion/2001. NACE International, Houston, p. 1-29 (2001).

5.   D.S. Dunn, G.A. Cragnolino, and N. Sridhar, Corrosion, 56 (2000) 90.

6.   A. Anderko and R.D. Young, Corrosion, 56 (2000) 543.

7.   A. Anderko, P. McKenzie and R.D. Young, Corrosion, 57 (2001) 202.

8.   N. Sridhar, C.S. Brossia, D.S. Dunn, J.P. Buckingham and A. Anderko, CORROSION/2002, paper no. 02204, NACE International, Houston (2002).

9.   N. Sridhar and G.A. Cragnolino, Corrosion, 49 (1993) 885.

10.   D.S. Dunn, N. Sridhar, and G.A. Cragnolino, Effect of Surface Conditions on Localized Corrosion of a Candidate High-Level Nuclear Waste Container Material, in: Proc. 12th Int. Corrosion Congress, NACE International, Houston, Texas, 1993, p. 4021.

11.   V. Jain, D.S. Dunn, N. Sridhar, and L.T. Yang, CORROSION/2003, Paper No. 03690. NACE International, Houston, (2003).

12.   A. Anderko and N. Sridhar, CORROSION/2001. Paper No. 1348. Houston, TX: NACE International (2001).

13.   T. Okada, J. Electrochem. Soc., 131 (1984) 1026.

14.   A. Anderko, N. Sridhar, C.S. Brossia, D.S. Dunn, L.T. Yang, B.J. Saldanha, S.L. Grise and M.H. Dorsey, CORROSION/2003, paper no. 03375, Houston, TX: NACE International (2003).

15.   Y.A. Popov and S.N. Sidorenko, "Theory of Interaction of Metals and Alloys with a Corrosive Environment", Cambridge International Science Publishing, Cambridge, UK (1998).

16.   H.K. Yashiro, S. Tanno, S. Koshiyama and K. Akashi, Corrosion 52(2) (1996) 109-114.

17.   J. Kolts and N. Sridhar, Temperature Effect in Localized Corrosion, in Corrosion of Nickel Base Alloys, ed. By R.C. Scarberry, ASM, 1984.

18.   E.L. Hibner, CORROSION/86, paper no. 181, Houston, TX: NACE International.

19.   T. Nakayama and K. Sasa, Corrosion, 32 (1976) 283.

20.   H. Yashiro and K. Tanno, Corros. Sci. 31 (1990) 485.

21.   N.G. Thompson and B.C. Syrett, Corrosion, 48 (1992) 649.

22.   K. Sugimoto and K. Asano, Analysis of Localized Corrosion on Stainless Steel by Microcomplex pH-pCl Electrode, in: H. Isaacs, V. Bertocci, J. Kruger, and S. Smialowska (Eds.), Advances in Localized Corrosion, NACE International, Houston, Texas, 1990, p. 375.

23.   N. Sridhar, Advances in Localized Corrosion, H.S. Isaacs, U. Bertocci, J. Kruger, and S. Smialowska (editors), Houston, TX: NACE International, p.263, (1990).

24.   E.L. Hibner, Materials Performance, 26 (3), pp. 37-40, (1987).

APPENDIX A: Special cases of the repassivation potential model

If only one aggressive species (e.g., Cl⁻) is present in the solution, eq. (40) simplifies to

$$1 + \left(\frac{i_{rp}}{i_p} - 1 \right) \frac{l_{H_2O}{''}}{i_{rp}} \exp\left(\frac{\xi_{H_2O} FE_{rp}}{RT} \right) = \frac{k_{Cl}{''}}{i_{rp}} \theta_{Cl}^{n_{Cl}} \exp\left(\frac{\alpha_{Cl} FE_{rp}}{RT} \right) \tag{A-1}$$

where α_{Cl} is assumed to be equal to 1. Thus, the system is characterized by two parameters that are specific to water-metal interactions (i.e., $l_{H_2O}{''}$ and ξ_{H_2O}) and two parameters that are specific to chloride-metal interactions (i.e., $k_{Cl}{''}$ and n_{Cl}). The i_{rp} and i_p parameters are universal for a given metal and denote the current density at which the repassivation potential is measured (typically 10^{-2} A·m⁻²) and the passive current density, respectively. If an additional aggressive species (e.g., Br⁻) is present, the right-hand side of eq. (A-1) is extended to include another term, i.e.,

$$1 + \left(\frac{i_{rp}}{i_p} - 1 \right) \frac{l_{H_2O}{''}}{i_{rp}} \exp\left(\frac{\xi_{H_2O} FE_{rp}}{RT} \right) = \frac{k_{Cl}{''}}{i_{rp}} \theta_{Cl}^{n_{Cl}} \exp\left(\frac{\alpha_{Cl} FE_{rp}}{RT} \right) + \frac{k_{Br}{''}}{i_{rp}} \theta_{Br}^{n_{Br}} \exp\left(\frac{\alpha_{Br} FE_{rp}}{RT} \right) \tag{A-2}$$

Thus, the additional parameters are $k_{Br}{''}$ and n_{Br}. If an inhibitive species (e.g., NO₃⁻) is present in the system rather than an additional aggressive species, the effect of the inhibitor is included on the left-hand side of eq. (A-1), i.e.,

$$1 + \left(\frac{i_{rp}}{i_p} - 1 \right) \frac{l_{H_2O}{''}}{i_{rp}} \exp\left(\frac{\xi_{H_2O} FE_{rp}}{RT} \right) + \left(\frac{i_{rp}}{i_p} - 1 \right) \frac{l_{NO_3}{''}}{i_{rp}} \theta_{NO_3}^{n_{NO3}} \exp\left(\frac{\xi_{NO_3} FE_{rp}}{RT} \right) = \frac{k_{Cl}{''}}{i_{rp}} \theta_{Cl}^{n_{Cl}} \exp\left(\frac{\alpha_{Cl} FE_{rp}}{RT} \right)$$

$$\tag{A-3}$$

where n_{NO_3} is assumed to be equal to 1. Then, the nitrate-specific parameters are $l_{NO_3}{''}$ and ξ_{NO_3}.

Table 1. Actual compositions of alloys tested in this study.

	Ni	Fe	Cr	Mo	C	Others
S41425	5.9	Bal.	12.1	1.9	0.01	
N06600	Bal.	8	15.5	0.0	0.15 max	
N10276	Bal.	5	15.5	16.0	0.01 max	W = 4
S31603	10	Bal.	17.0	2.5	0.03 max.	
S31254	18	Bal.	20.0	6.1	0.02 max.	N = 0.2; Cu = 0.7
N08367	25	Bal.	20.5	6.5	0.02 max.	N = 0.2
N08800	32.5	39.5	21.0	0.0	0.1 max	Cu = 0.75 max
N08825	42	29	21.5	3.0	0.05 max	Cu = 2.0
N06625	Bal.	5 max	21.5	9.0	0.1 max	Nb = 3.65
N06022	56	3	22.0	13.0	0.01 max	W = 3.0
N06690	Bal.	9	29.0	0.0	0.05 max	
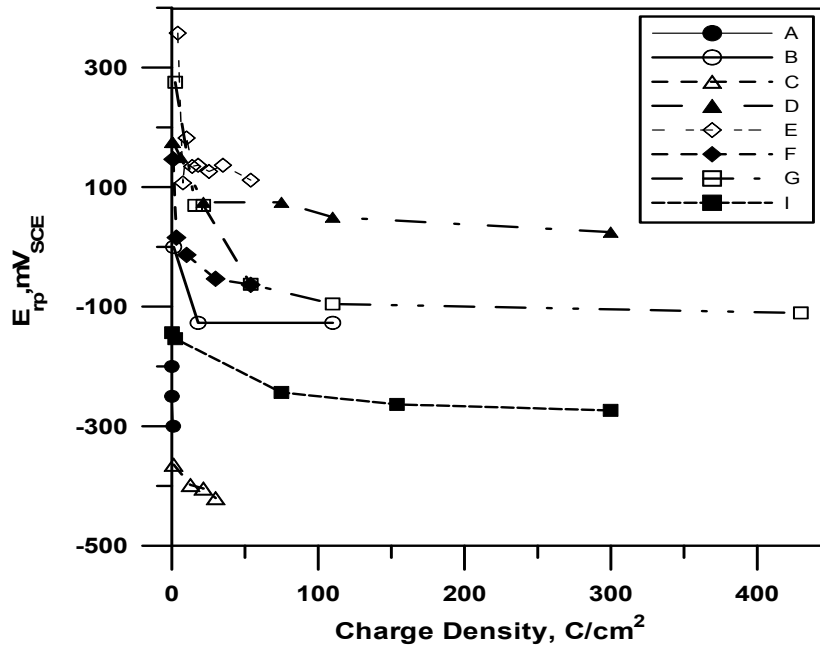
Figure 1. Effect of charge density (pit/crevice corrosion depth) on the repassivation potential showing attainment of a lower-bound value. Sources of data: A: Ref. 3; B: Ref. 19; C: Ref. 20; D: Ref. 21; E: Ref. 9; F: Ref. 9; G: Ref. 10; I: Ref.22. Note that the data pertain to different alloy-environment combinations and test techniques.
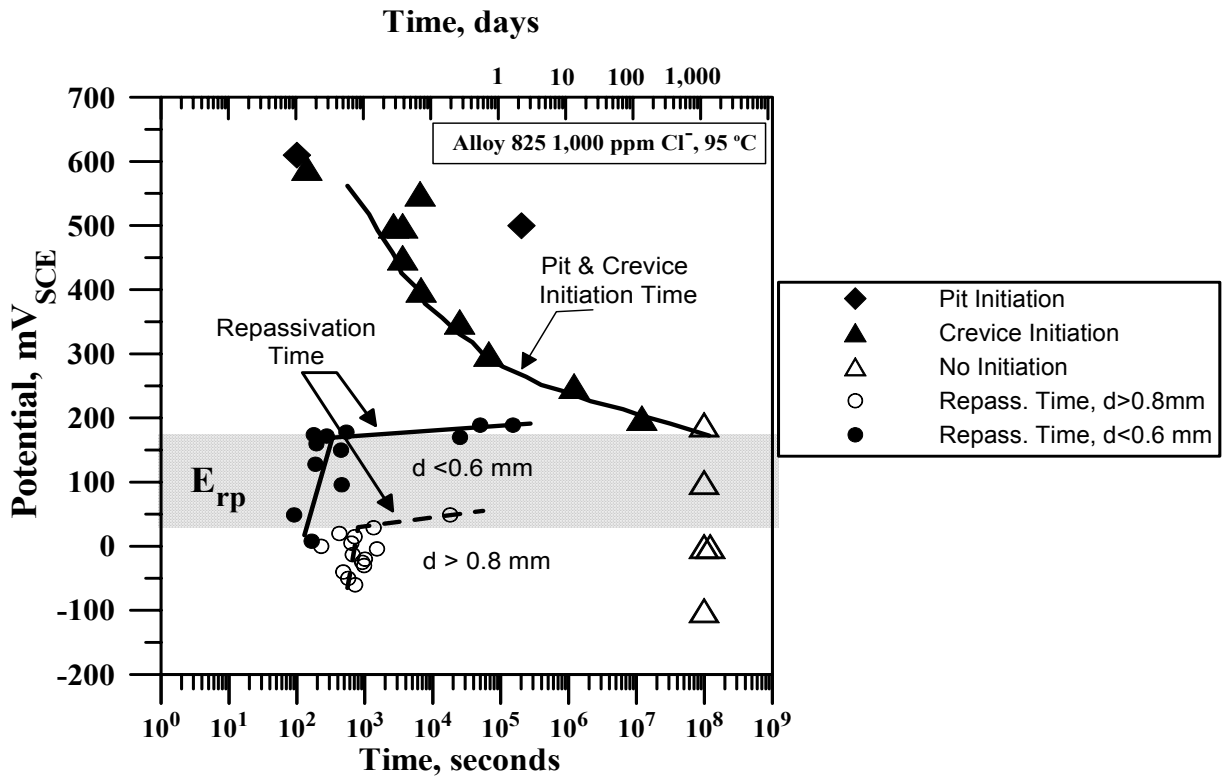
Figure 2. Effect of applied potential on the time to initiate stable pitting or crevice corrosion and on the time to repassivate stable crevice corrosion. For repassivation, two different populations of crevice depths (depth of corrosion perpendicular to the crevice surface) were considered by growing the corrosion for different time periods prior to repassivation.
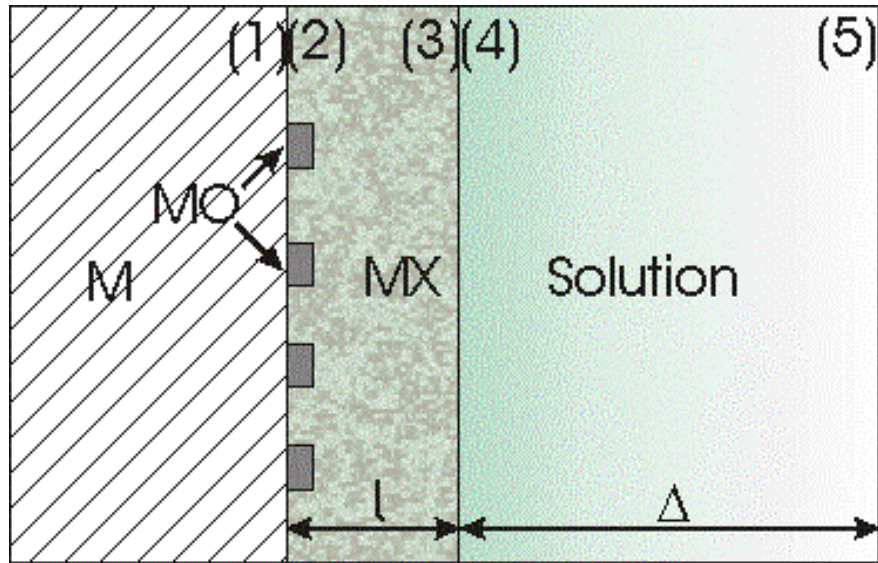
Figure 3. Schematic summary of the phases and interfaces considered in the derivation of the model (M - metal; MX – metal halide; MO – metal oxide; the numbers indicate the interfaces between the phases)
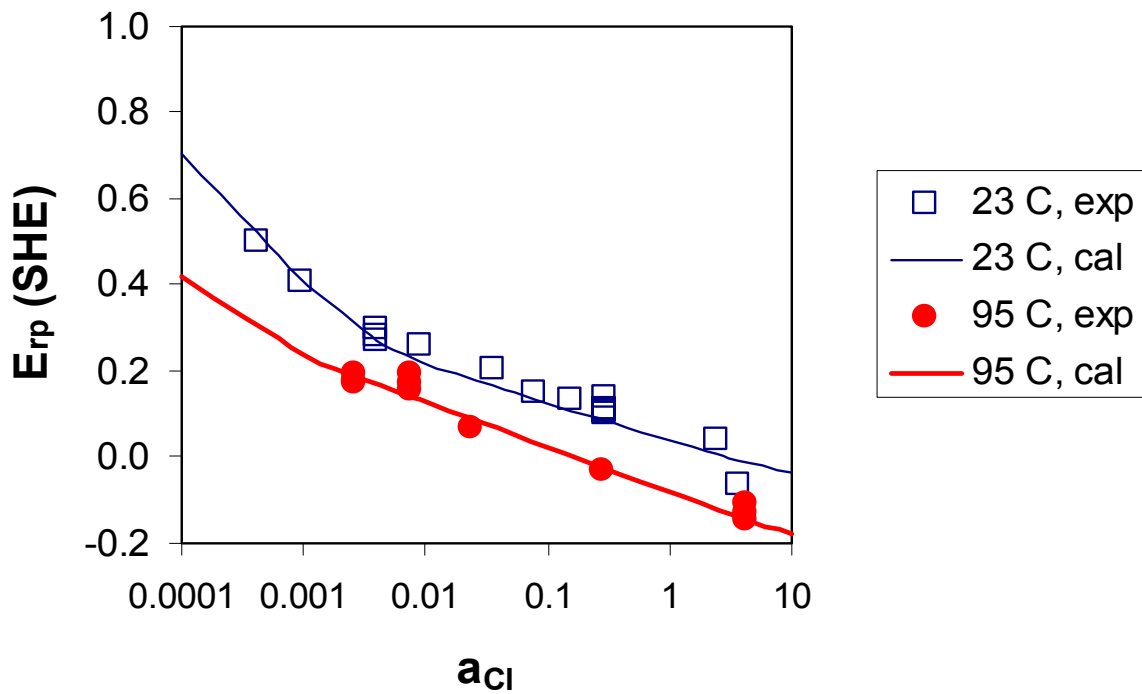
Figure 4. Calculated and experimental repassivation potentials for type 316L stainless steel (UNS S31603) at 23 °C and 95 °C as a function of chloride ion activity.
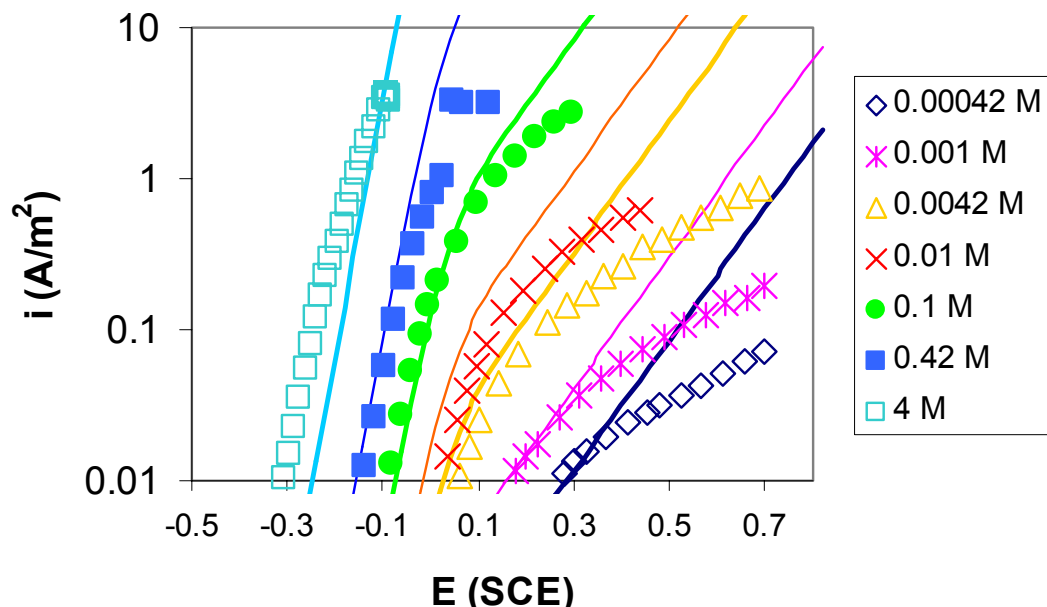
Figure 5. Limiting slopes of i(E) relationships prior to repassivation calculated from the model (lines) and obtained from experimental measurements (symbols) for type 316L stainless steel at 23 °C for selected chloride concentrations.
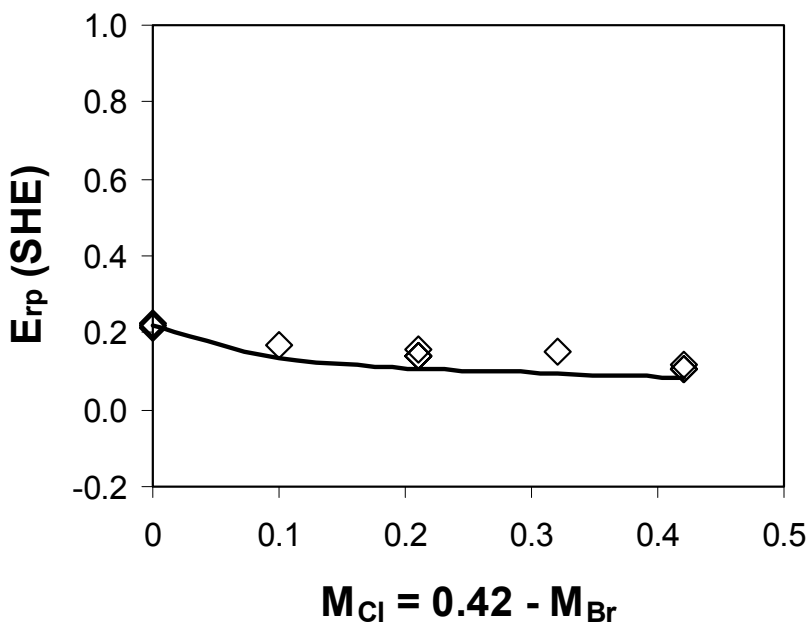
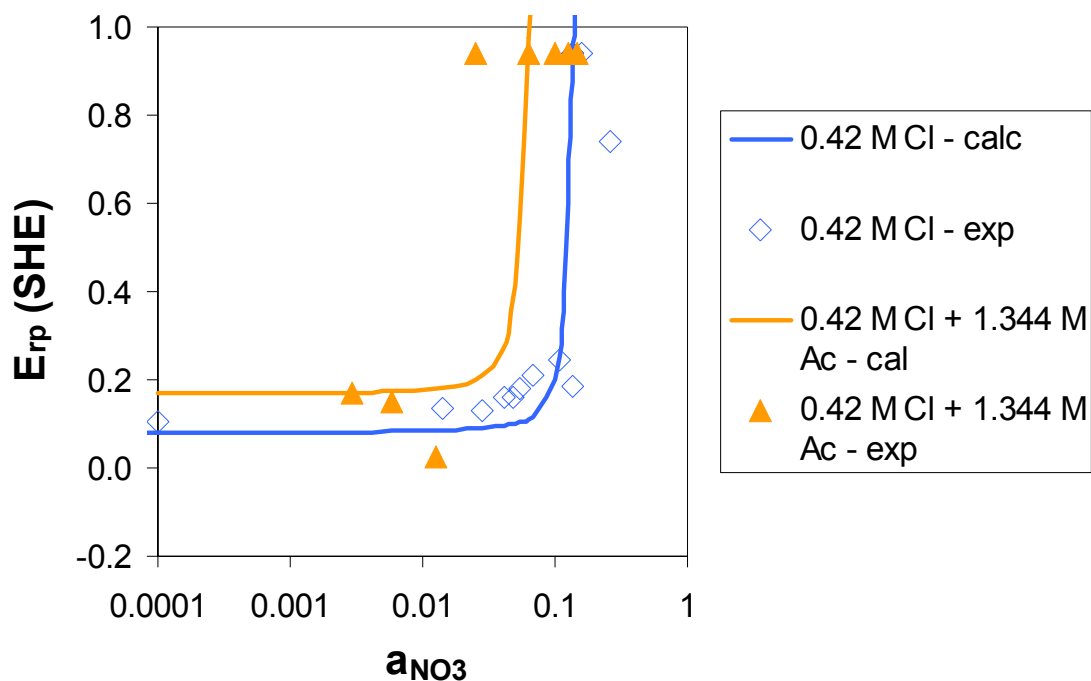**Figure 6. Calculated and experimental repassivation potentials for type 316L stainless steel in solutions containing chloride and bromide ions with a total molarity of 0.42 M.**
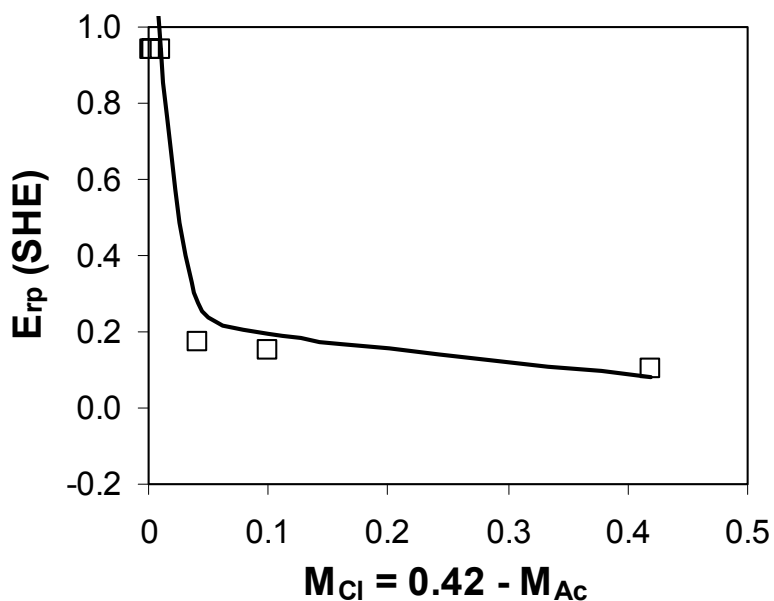
Figure 7. Calculated and experimental repassivation potentials for type 316L stainless steel in solutions containing chloride and acetate ions with a total molarity of 0.42 M.
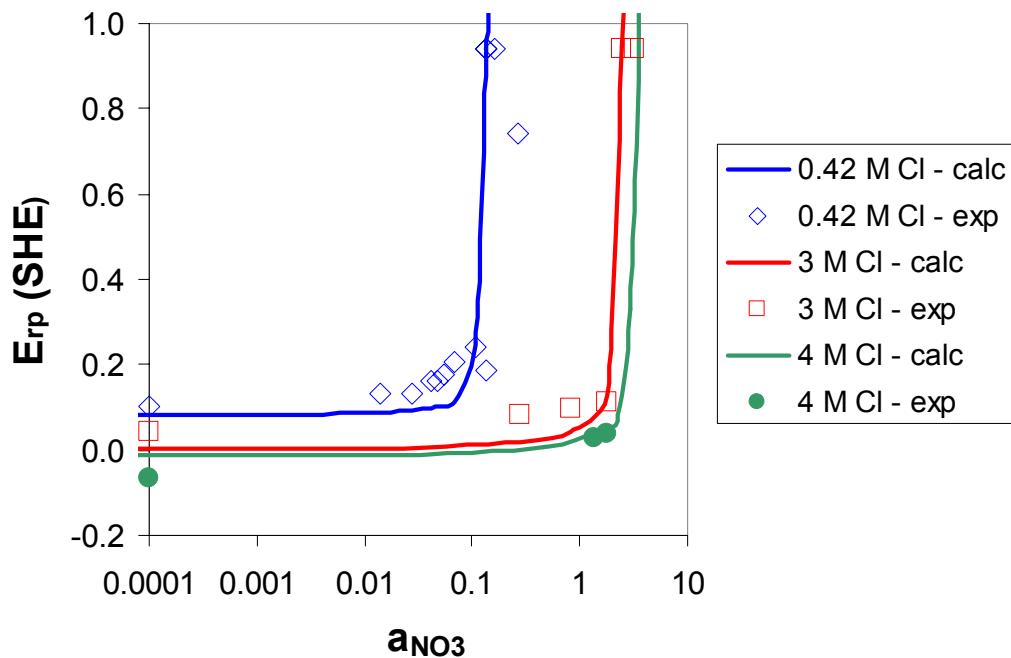
Figure 8. Calculated and experimental repassivation potentials for type 316L stainless steel in solutions containing chloride and nitrate ions as a function of nitrate ion activity for three concentrations of chloride.

Figure 9. Calculated and experimental repassivation potentials for type 316L stainless steel in solutions containing chloride, nitrate and acetate ions as a function of nitrate ion activity for systems with chloride concentrations fixed at 0.42 M and acetate concentrations equal to either 0 or 1.344 M.
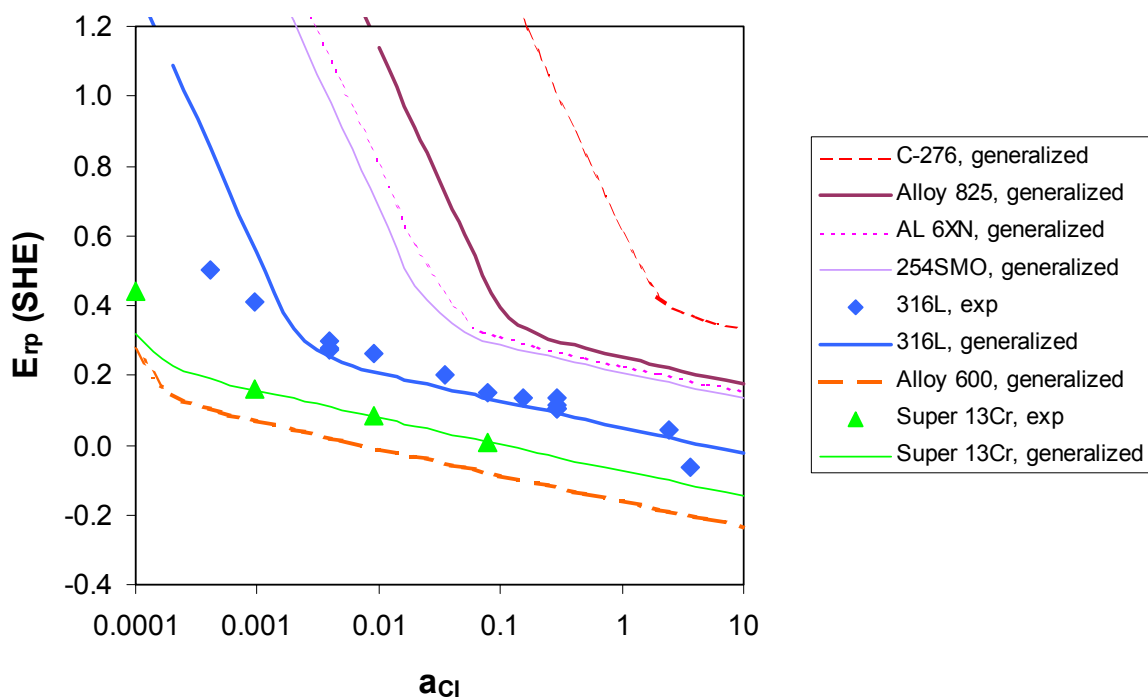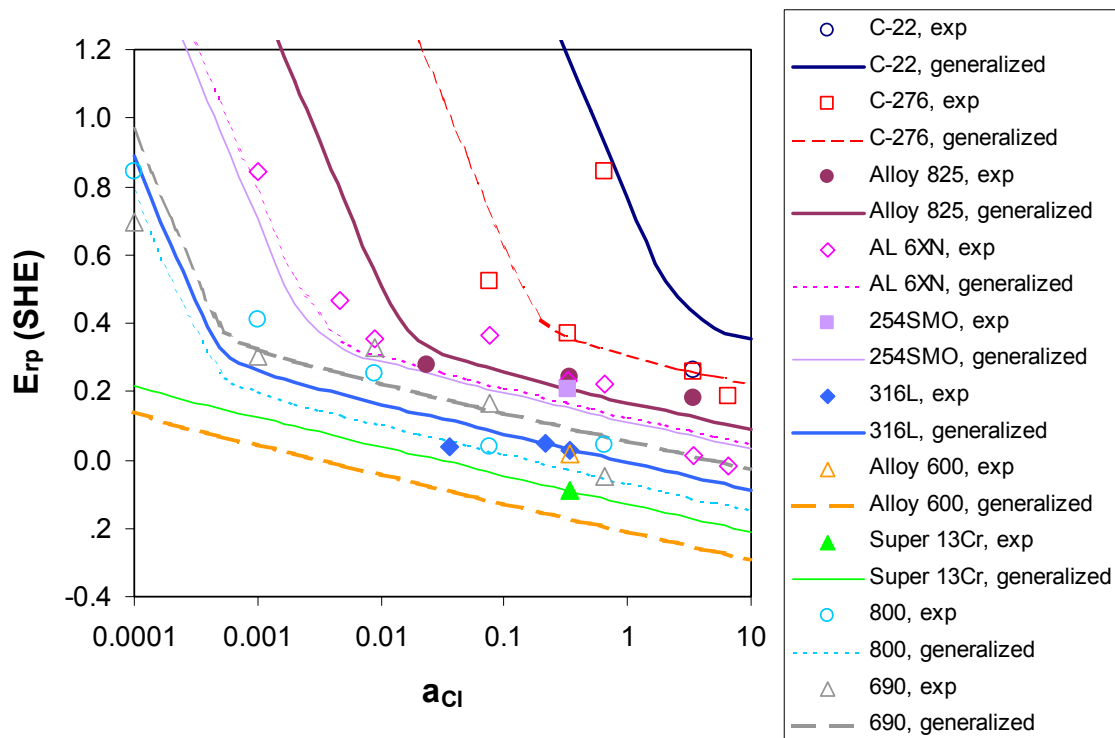

Figure 10. Calculated and experimental repassivation potentials for several alloys in chloride solutions at 296 K. The lines were obtained from the generalized correlation with alloy composition.

Figure 11. Calculated and experimental repassivation potentials for several alloys in chloride solutions at 333 K. The lines were obtained from the generalized correlation with alloy composition.
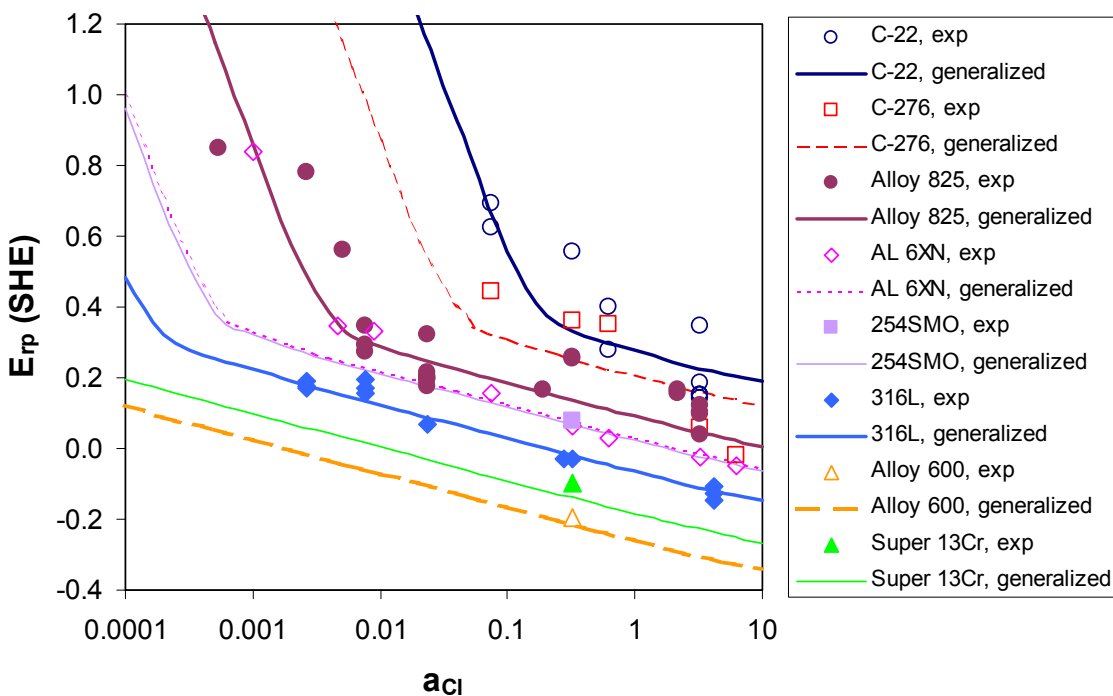

Figure 12. Calculated and experimental repassivation potentials for several alloys in chloride solutions at 368 K. The lines were obtained from the generalized correlation with alloy composition.
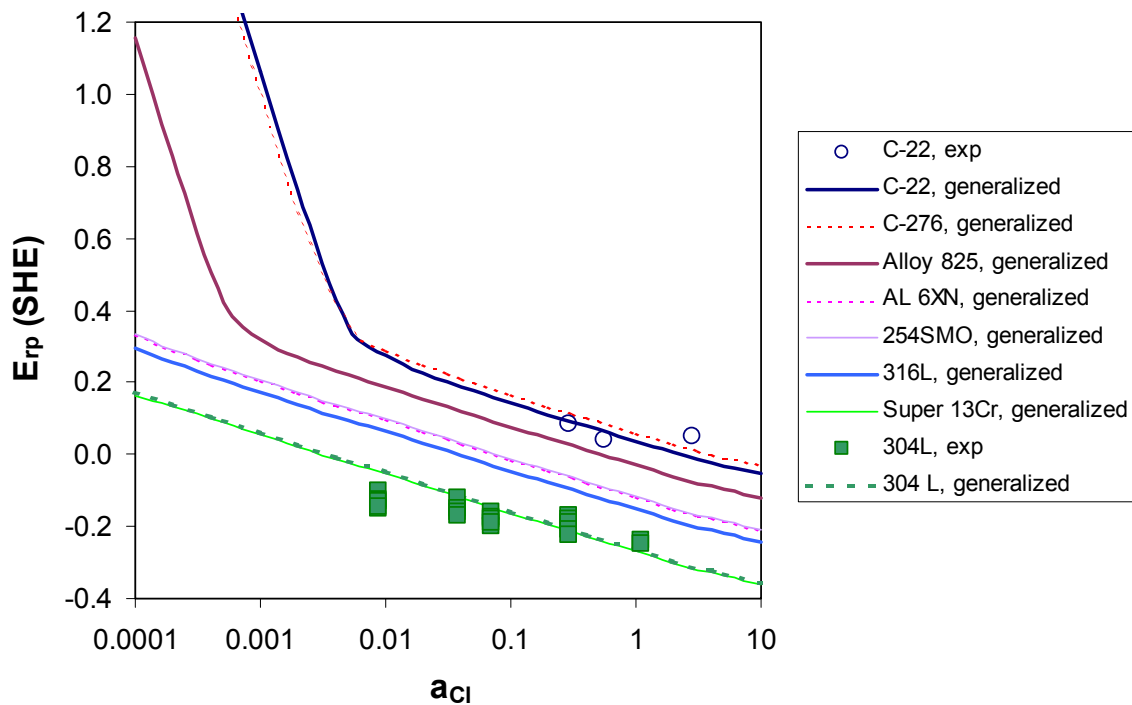
Figure 13. Calculated and experimental repassivation potentials for several alloys in chloride solutions at 423 K. The lines were obtained from the generalized correlation with alloy composition.
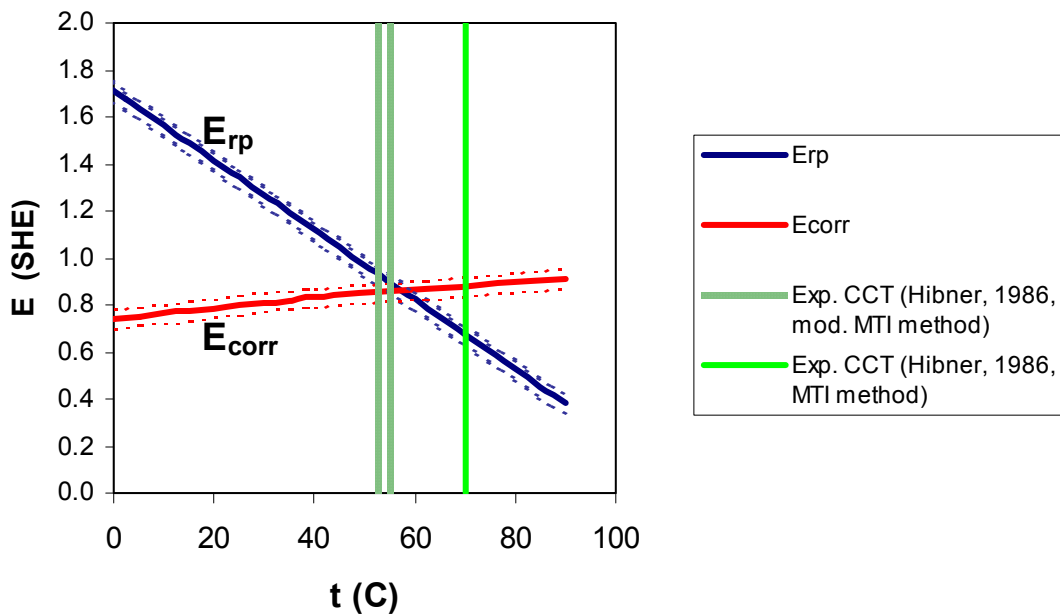

Figure 14. Prediction of the critical crevice temperature (CCT) for UNS N06022 in a 6% FeCl$_3$ solution. The vertical lines show the location of the experimental CCT values measured by Hibner[18] using various methods. The intersection of the calculated corrosion potential and repassivation potential lines shows the predicted critical crevice temperature.